

# Flexible Filter-Free Narrowband Photodetector with High Gain and Customized Responsive Spectrum

Liang Gao, Cong Ge, Wenhui Li, Chuancheng Jia, Kai Zeng, Weicheng Pan, Haodi Wu, Yang Zhao, Yisu He, Jungang He, Zhixin Zhao, Guangda Niu, Xuefeng Guo, F. Pelayo Garcia de Arquer, Edward H. Sargent, and Jiang Tang\*

Conventional narrowband photodetection is enabled by coupling broadband photodetectors with complex optical filters. The recently reported charge collection narrowing, an alternative filter-free strategy, attains very narrowband photodetection at the sacrifice of sensitivity. Herein, a new strategy is proposed to customize the responsive spectrum with high gain by using dye molecules with intrinsically versatile and narrowband absorption. The device configuration is organic dye/Zn<sub>0.9</sub>Mg<sub>0.1</sub>O nanoparticles/graphene, where the organic dye serves as the narrowband absorber, graphene serves as the fast carrier transport channel, and Zn<sub>0.9</sub>Mg<sub>0.1</sub>O nanoparticles play a triple role of enhancing dye loading, suppressing dye aggregation and blocking charge back recombination. A high responsivity of  $8 \times 10^3 \text{ A W}^{-1}$  is thus obtained at a 530 nm response peak with a 60 nm full-width at half maximum, a four orders of magnitude increase in sensitivity compared to the best narrowband photodetectors reported to date under the comparable electric field. Organic dyes with dual-band absorption to demonstrate narrowband photodetectors with customized responsive spectrum are further implemented. The approach opens the way to the realization of efficient flexible narrowband photodetection for electronic skin and wearable electronic applications.

## 1. Introduction

Photodetectors are widely employed as an essential part of imaging system, telecommunications, biological sensing, and environmental surveillance.<sup>[1–3]</sup> On the basis of their response spectrum, photodetectors can be approximately categorized as broadband<sup>[4–6]</sup> and narrowband.<sup>[7–9]</sup> Narrowband photodetection in state-of-the-art commercial application combines Si or InGaAs-based broadband photodetector with a set of interference filters to allow response toward a small targeted spectrum.<sup>[10]</sup> However, these filters not only

increase the photodetector cost and limit pixel density in imaging system, but also would lose their functions in the curved circumstances as their interference effect depends heavily on the optical path difference (OPD).<sup>[11]</sup>

Filter-free narrowband photodetectors have therefore attracted great research interest in recent years. Plenty of alternative strategies have emerged for filter-free narrowband photodetectors, including (1) intentionally enhancing light absorption of particular wavelength via the plasmonic effect;<sup>[7]</sup> (2) controlling sub-band enhanced light absorption within the active layer through an optical structure design;<sup>[12]</sup> (3) using wide-bandgap semiconductors with limited responsive spectrum as the absorbers;<sup>[13,14]</sup> and (4) taking advantage of the charge collection narrowing (CCN) to manipulate the external quantum efficiency (EQE) of the photodiodes.<sup>[15–18]</sup> However, all are not perfect. The plasmonic enhanced absorption (the first strategy)

is limited to specific spectral range and has difficulties to be widely tunable. The optical manipulation (the second strategy) faces the same challenge as the filters, such as complex configuration and high cost. As for wide-bandgap semiconductors (the third strategy), despite their successful use for narrowband ultraviolet detection, it remains impracticable to realize narrowband visible or infrared detection. Among these strategies, CCN (the fourth one) has thus far resulted in the narrowest photoreponse. This approach, however, relies on a recombination loss by which only a small fraction of incident photons with energies close to the bandgap of the material are absorbed in the bulk

L. Gao, C. Ge, K. Zeng, W. Pan, H. Wu, Y. Zhao, Y. He, Dr. J. He, Prof. Z. Zhao, Prof. G. Niu, Prof. J. Tang  
Wuhan National Laboratory for Optoelectronics (WNLO)  
and School of Optical and Electronic Information  
Huazhong University of Science and Technology (HUST)  
Wuhan 430074, China  
E-mail: jtang@mail.hust.edu.cn

Prof. W. Li  
School of Information Engineering  
Jiangxi University of Science and Technology  
Ganzhou 341000, China

Prof. C. Jia, X. Guo  
Beijing National Laboratory for Molecular Sciences  
State Key Laboratory for Structural Chemistry of  
Unstable and Stable Species  
College of Chemistry and Molecular Engineering  
Peking University  
Beijing 100871, China

Dr. F. P. Garcia de Arquer, Prof. E. H. Sargent  
Department of Electrical and Computer Engineering  
University of Toronto  
10 King's College Road, Toronto, Ontario M5S 3G4, Canada

DOI: 10.1002/adfm.201702360

and collected efficiently, leading to narrowband photoresponse with compromised responsivity. Accordingly, it still remains a grand challenge to build sensitive narrowband photodetectors with widely tunable responsive spectrum.

We note that organic dye molecules are one unique class of intrinsically narrowband absorbers with high absorption coefficients, stemming from their well-defined isolated energy levels.<sup>[19,20]</sup> Moreover, there are a myriad of dyes with narrowband absorption in nature, and some even demonstrate response to multiple isolated section of the solar spectrum.<sup>[21]</sup> These properties render organic dyes, in principle, as ideal candidates for narrowband photodetection. Two main challenges have not precluded thus far the translation of these features into efficient photodetection: first, the limited carrier mobility of dye molecules poses difficulties to their direct integration as active layers in optoelectronic devices;<sup>[22]</sup> second, as they assemble into films, the electronic interactions between dye aggregates, and/or between dyes molecules and adjacent materials hybridize their energy levels and in turn widen the absorption spectra.<sup>[23,24]</sup> In order to overcome the impractically low mobility of dye molecules, we turned our attention to a graphene hybrid architecture whereby photoexcited carriers in the dye molecules are injected into the fast graphene transport channel.<sup>[25]</sup> This strategy, however, results in a broadening of the response due to the dye molecule conjugation and the  $\pi$ -bond resonance between dye molecules and graphene.<sup>[26]</sup> We proposed that sandwiching a metal oxide nanoparticles layer between the dyes and the graphene channel could kill two birds with one stone: first, dye molecules could anchor to the surface of nanoparticles, increasing the absorption significantly, akin to the dye-sensitized solar cells; second, these dyes are organized in a 3D space on the spherical surface of nanoparticles with minimized overlapping, and thus alleviate linewidth broadening.<sup>[27–29]</sup>

Following these designing rules, herein we demonstrated a sensitive and narrowband hybrid photodetector using the organic dyes as the narrowband absorber and graphene as the carrier transport channel. A sandwiched  $\text{Zn}_{0.9}\text{Mg}_{0.1}\text{O}$  nanoparticle buffer layer was employed to suppress the dye molecule conjugation and the  $\pi$ -bond resonance between dye molecule and graphene, and also serves as the relay layer for charge transfer. Dictated by the absorption of a small BODIPY sensitizer (BET) dye, the hybrid BET/ $\text{Zn}_{0.9}\text{Mg}_{0.1}\text{O}$  nanoparticles/graphene (BZG) photodetector showed photoresponse in 470–580 nm range with a peak responsivity of  $8 \times 10^3 \text{ A W}^{-1}$ . Similarly, another hybrid dye molecule (N4)/ $\text{Zn}_{0.9}\text{Mg}_{0.1}\text{O}$  nanoparticles/graphene (NZG) device realized narrowband photodetection at 400–500 nm and 610–700 nm, consistent with the absorption spectrum of N4 molecules. Furthermore, our narrowband BZG photodetectors exhibited excellent flexibility, while commercial narrowband photodetector using the interference filter completely lost its function. Our work thus highlighted the great potential of using dyes for sensitive narrowband photodetectors, particularly for those requiring flexibility and customized responsive spectrum.

## 2. Results and Discussion

We took a small BODIPY sensitizer (BET) as a sample to explain how the aggregation of dye molecules affects their light

absorption, especially the absorption breadth in **Figure 1**. The BET is a boron dipyrromethene compound with one benzoic acid group and two ethyl groups.<sup>[30]</sup> The energy level of an isolated BET molecule is discrete, as shown in **Figure 1a**, which leads to narrowband absorption in **Figure 1d** corresponding to optical transition between the energy gap.<sup>[31]</sup> For BET in toluene, its specific absorption ranges from 450 to 550 nm, and the full width at half maximum (FWHM) is about 46 nm. **Figure 1b** shows the BET/graphene hybrid structure, in which the  $\pi$ -bond resonance<sup>[25,32]</sup> between planar BET molecule and graphene broadens the absorption. While many BET molecules couple together to form a long-range-ordered morphological structure in **Figure 1c**, the delocalization of electrons among the whole aggregate causes the discrete levels of each isolated molecule to overlap and split into a huge number of energy levels forming band-like states.<sup>[33]</sup> As a result, the absorption of BET molecule aggregate is much wider than that of an isolated BET molecule. As a strong evidence, the absorption of BET on graphene in **Figure 1e** is extended to infrared range by the  $\pi$ -bond resonance between graphene and BET molecule, and its FWHM is broadened in a large scale to about 100 nm by the coupling of BET molecule.<sup>[25,33]</sup> In order to take advantage of the narrowband absorption of dye molecule in the sensitized graphene system, the  $\pi$ -bond resonance between dye molecule and graphene as well as dye molecule coupling should be minimized.

A novel BZG hybrid structure in **Figure 1f** was constructed for narrowband photodetection, in which isolated BET molecules were anchored onto  $\text{Zn}_{0.9}\text{Mg}_{0.1}\text{O}$  nanoparticles to keep narrowband absorption. The few-layer graphene was grown by a modified chemical vapor deposition (CVD) method and transferred onto a glass substrate through the method of Guo and co-workers.<sup>[34]</sup> A  $\approx 60 \text{ nm}$  thick  $\text{Zn}_{0.9}\text{Mg}_{0.1}\text{O}$  nanoparticles layer was deposited on graphene with full coverage by the spin-coating method, as shown in **Figures S1 and S2** (Supporting Information). The  $\text{Zn}_{0.9}\text{Mg}_{0.1}\text{O}$ /graphene were then soaked in a  $0.17 \text{ mg mL}^{-1}$  BET toluene solution for an optimized time of 30 min (**Figures S3 and S4**, Supporting Information) and then rinsed by toluene to keep chemically absorbed BET molecules and remove physically absorbed BET molecules. In the BZG hybrid structure, graphene acts as a charge transport channel, the  $\text{Zn}_{0.9}\text{Mg}_{0.1}\text{O}$  nanoparticles layer serves as a wide-bandgap buffer layer, and BET plays the role of light absorber. The benzoic acid group of BET molecule prompts its binding to the active sites on the surface of  $\text{Zn}_{0.9}\text{Mg}_{0.1}\text{O}$  nanoparticles.<sup>[26,35,36]</sup> So the chemical-bonded BET molecules would remain tightly anchored onto the  $\text{Zn}_{0.9}\text{Mg}_{0.1}\text{O}$  layer, while the free BET molecules, as well as BET aggregates loosely sitting on the  $\text{Zn}_{0.9}\text{Mg}_{0.1}\text{O}$  layer could be washed out by toluene, a good solvent of BET. It should be emphasized that the  $\text{Zn}_{0.9}\text{Mg}_{0.1}\text{O}$  nanoparticles layer brings three benefits. First, it helps to preserve the narrowband absorption nature of BET dyes because it not only prevents the direct contact between BET molecule and graphene that broadens absorption due to the  $\pi$ -bond resonance, but also minimizes dye coupling thanks to its spherical morphology. Second, the large surface area increases the loading of dye molecules, enhancing light absorption and consequently photoresponse. Third, it assists the injection of photogenerated carriers from dyes into graphene-transporting

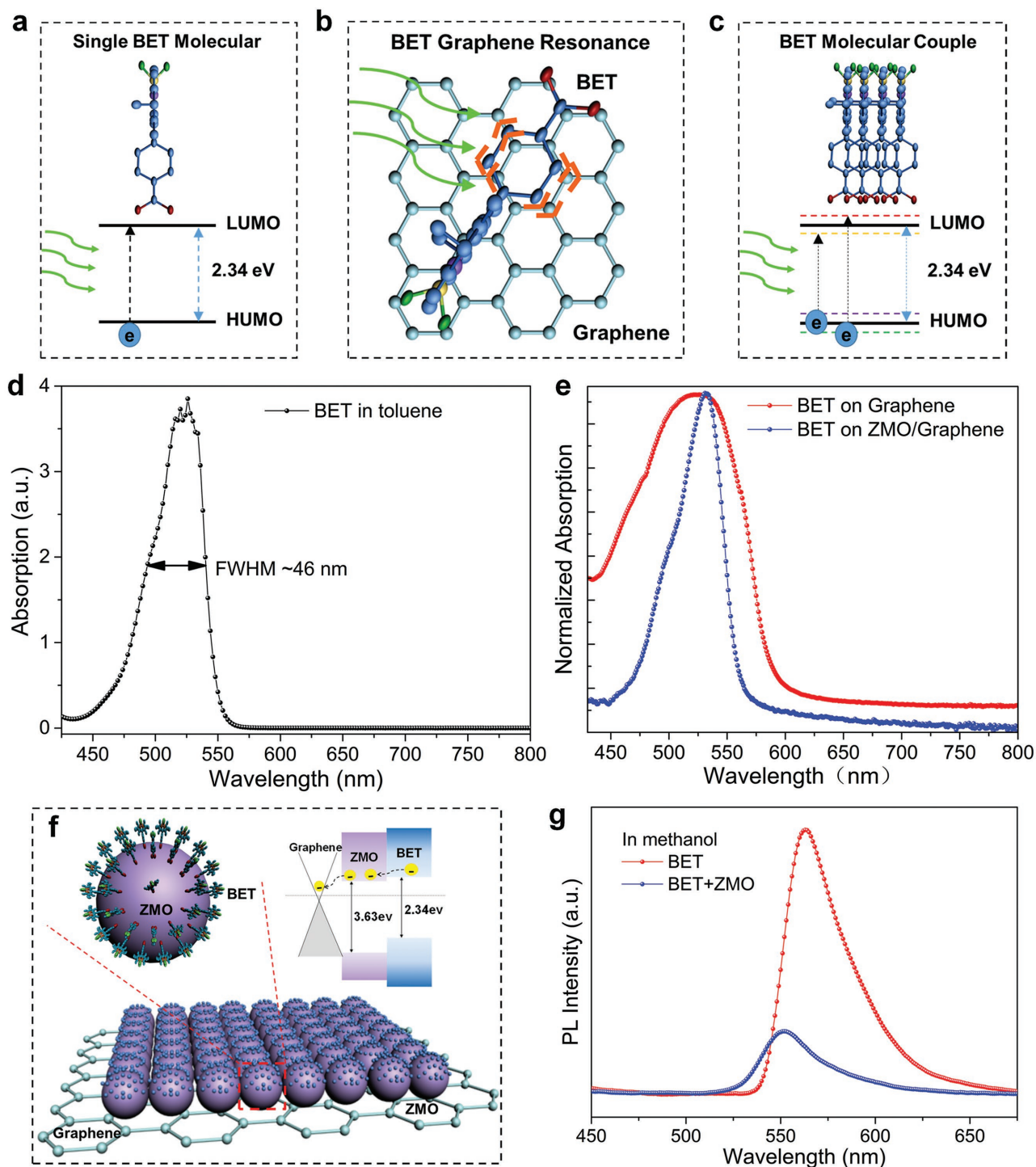


**Figure 1.** BET molecule structures resulting in different light absorption. a) Single BET molecule with discrete energy level. b) BET and graphene structure with resonance absorption. c) BET molecular couple with continuous energy band. d) Absorption of dispersed BET molecule in toluene. e) Absorption of BET on graphene and on the  $Zn_{0.9}Mg_{0.1}O$ /graphene structure. f) Cross-section and enlarged top views of the BZG structure. The right inset is band alignment of the BZG structure. g) Photoluminescence (PL) spectra of BET and BET with  $Zn_{0.9}Mg_{0.1}O$  nanoparticles in methanol. The BET concentration is the same.

channel and blocks detrimental recombination loss between electrons in graphene and residual holes in the dyes, as per the band diagram shown in the inset of Figure 1f. Hence, this BZG hybrid structure could take full advantage of the

intrinsically narrowband light absorption of BET molecules. The normalized absorption of the BZG hybrid structure in Figure 1e exhibits the absorption range covering from 450 to 550 nm, with its absorption peak at 530 nm and the FWHM of

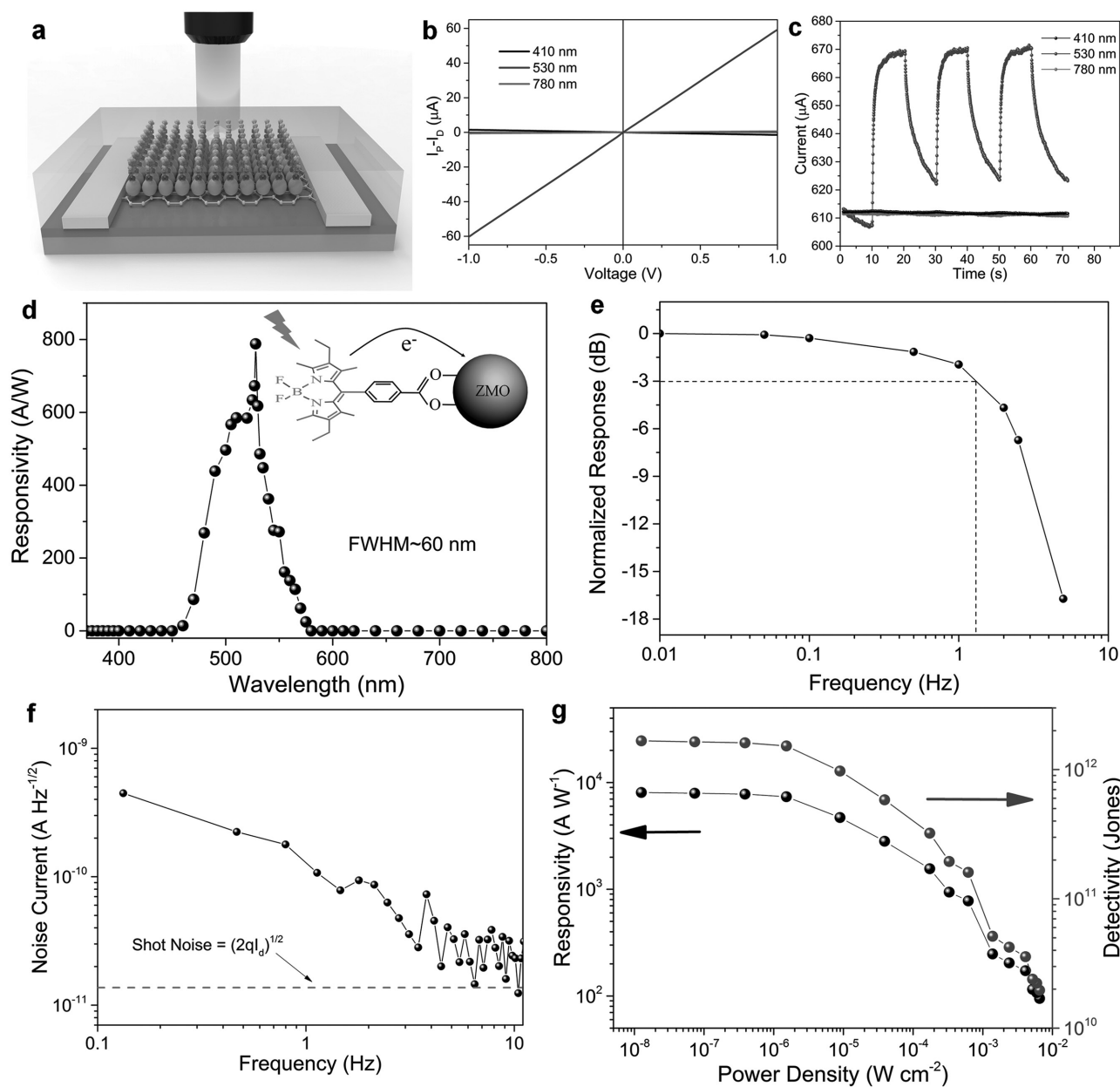


**Figure 2.** Narrowband photodetection of the BZG device with polymethyl methacrylate (PMMA) encapsulation. a) Device structure, b) current–voltage ( $I$ – $V$ ) curves, and c) transient response ( $I$ – $t$ ) under illumination with different wavelength. d) Responsivity as a function of incident wavelength. The inset shows the intrinsic narrowband absorption of BET molecule caused by its two ethyl groups. e) Frequency response, f) measured current noise at different frequency, and g) measured responsivity and specific detectivity at 1 Hz as a function of 530 nm light power density of PMMA-encapsulated BZG device.

about 50 nm. Upon illumination, photogenerated electrons are transferred from BET to  $\text{Zn}_{0.9}\text{Mg}_{0.1}\text{O}$  nanoparticles through the anchoring group, and then injected into graphene. We measured the photoluminescence (PL) spectra of two BET methanol solutions with the same concentration, one of which contained  $\text{Zn}_{0.9}\text{Mg}_{0.1}\text{O}$  nanoparticles. The apparent PL quenching of the BET solution containing  $\text{Zn}_{0.9}\text{Mg}_{0.1}\text{O}$ , as shown in Figure 1g, confirms efficient charge transfer from BET molecule to  $\text{Zn}_{0.9}\text{Mg}_{0.1}\text{O}$  nanoparticles. The PL remnants could be originated from free BET molecules, and the blue shift of PL

peak was ascribed to the inner electronic structure change of BET molecule after anchored on  $\text{Zn}_{0.9}\text{Mg}_{0.1}\text{O}$  nanoparticles.<sup>[37]</sup>

Excellent narrowband photodetection of BZG device is displayed in Figure 2. Devices were constructed onto a silicon wafer with 300 nm  $\text{SiO}_2$  layer. And the Au electrodes were deposited by thermal evaporation and patterned by a designed mask with a length of 10  $\mu\text{m}$  and a width of 0.5 mm. Finally, the whole BZG device was encapsulated by polymethyl methacrylate (PMMA) using the spin-coating method. PMMA encapsulation minimized interference from absorbed gas molecules

such as H<sub>2</sub>O and O<sub>2</sub> from the environment and improved device reproducibility (Figure S5, Supporting Information). Current–voltage (*I*–*V*) curves of this device were tested under 410, 530, and 780 nm monochromatic illumination, with the power density all kept identical at 1.36 mW cm<sup>-2</sup>. The gain current, the difference between photocurrent (*I<sub>p</sub>*) and dark current (*I<sub>D</sub>*), as a function of external bias is shown in Figure 2b. Linear *I*–*V* curves (Figure S6, Supporting Information) were obtained, suggesting the expected good contact between Au electrodes and graphene.<sup>[38]</sup> The BZG hybrid photodetector had strong response to 530 nm light but no response to 410 and 780 nm light. This spectrally selective detection is further confirmed by transient response (*I*–*t* curves) to different light in Figure 2c. The *I*–*t* curve to 530 nm light presents obvious regular fluctuation along with light on and off, but the other two *I*–*t* curves under 410 and 780 nm illumination demonstrate no photoresponse at all. The response is somewhat sluggish and could be improved by a gate voltage pulse (Figure S7, Supporting Information), in analogy to the MoS<sub>2</sub> and In<sub>2</sub>Se<sub>3</sub> phototransistor.<sup>[39,40]</sup> Figure 2d shows the specific response range of the BZG hybrid photodetector. The responsivity is calculated by the equation  $R = (I_p - I_D)/P_{in}$ , where *P<sub>in</sub>* is the incident light power, the product of incident light power density and active area of the device. The responsivity to different monochromatic light (its intensities during the measurement were at dozens μW cm<sup>-2</sup> as shown in Figure S9 in the Supporting Information) is very similar to the absorption spectrum of BET molecule on Zn<sub>0.9</sub>Mg<sub>0.1</sub>O nanoparticles in Figure 1e. The response range covers from 450 to 580 nm, and the peak responsivity is about 800 A W<sup>-1</sup> at 530 nm. The FWHM is about 60 nm, which is comparable with that of other narrowband photodetectors as listed in **Table 1**. Importantly, the responsivity or EQE (Figure S8, Supporting Information) is thousands of times that of the reported narrowband photodetectors under the same electric field. In comparison, the perovskite single-crystal narrowband photodetectors employ surface defects to recombine whole carriers generated from short wavelength light and majority of carriers from the target light, realizing narrowband photodetection but

leading to rather low responsivity and EQE. The sensitivity of our narrowband photodetector is unprecedentedly high for three reasons: one is the extreme strong absorption nature of dye molecules, the other reason is the significantly enhanced dye loading onto the Zn<sub>0.9</sub>Mg<sub>0.1</sub>O nanoparticle, and the third one is the ultrafast charge transport along the graphene channel inherited from the sensitized graphene photoconductive detector.<sup>[6,39]</sup> All the three features added up, leading to more sensitive narrowband photodetection than the preceding photodetectors reported in the literature.

In order to further exhibit the performance of our BZG narrowband photodetector, the frequency-dependent photoresponse is displayed in Figure 2e, and the transient responses to illumination with different power density are shown in Figure S10 (Supporting Information). The 3 dB bandwidth of our BZG device is ≈1 Hz due to the long recombination time of photogenerated holes and electrons. The noise current in Figure 2f declines linearly with the frequency between 0.1 and 10 Hz, containing strong 1/*f* noise component. The red dash line in Figure 2f indicates estimated shot noise, calculated from dark current. Figure 2g displays responsivity (*R*) and detectivity (*D*<sup>\*</sup>) of our PMMA-encapsulated BZG photodetector under 530 nm monochromatic illumination with the power density varying from 1 μW cm<sup>-2</sup> to 50 mW cm<sup>-2</sup>. Detectivity, the integrated figure of merit to compare device performance between various photodetectors is calculated as  $D^* = R\sqrt{A}f/i_n$ , where *A* is the device active area, *f* is the frequency bandwidth, and *i<sub>n</sub>* is the noise current. Because of the gradual filling of high-gain deep defects along with the increase of incident light intensity, responsivity and detectivity both decrease gradually<sup>[41,42]</sup> upon strong illumination, a general observation for photoconductive photodetectors. Under 10<sup>-8</sup> W cm<sup>-2</sup> weak illumination, the responsivity and EQE reach up to 8 × 10<sup>3</sup> A W<sup>-1</sup> and 1.87 × 10<sup>4</sup>, respectively, which are the highest among the reported filter-free narrowband photodetectors as summarized in Table 1. Such a high sensitivity is mainly attributed to the long carrier lifetime and the ultrafast carrier transit in the photoconductor structure,<sup>[6,43]</sup> as

**Table 1.** Performance comparison between representative filter-free narrowband photodetectors. “–” means “not given”.

Ref.	Strategy	Response peak [nm]	FWHM [nm]	Electric field [V μm <sup>-1</sup> ]	EQE	Detectivity [Jones]
[13]	Al <sub>x</sub> Ga <sub>1-x</sub> N	275	≈12.5	3.2	89%	–
[19]	Organic	525	90	14	17%	10 <sup>11</sup>
[20]	Organic	550	≈150	41	60.7%	–
[7]	Plasmon	1460	≈100	0	≈0.051%	–
[12]	Optical Design	≈460	–	0	8%	–
[15]	CCN	Visible	<20	0.08	1.6%	2 × 10 <sup>10</sup>
[16]	CCN	Visible	<100	1	12%	2 × 10 <sup>11</sup>
[17]	CCN	Red and near IR	<90	0.33	35%	5 × 10 <sup>12</sup>
[18]	CCN	650	<30	4	49%	1.35 × 10 <sup>11</sup>
				24	5.35 × 10 <sup>4</sup>	–
This work	BZG	530	≈50	0.1	1.87 × 10 <sup>4</sup>	1.7 × 10 <sup>12</sup>
This work	NZG	460	≈50	0.1	1.75 × 10 <sup>4</sup>	1.3 × 10 <sup>12</sup>
		660	≈45		3.66 × 10 <sup>3</sup>	4 × 10 <sup>11</sup>

photodetector gain (or EQE) is decided by the division of carrier lifetime and transit time.<sup>[44]</sup> The photogenerated electrons contribute to the photocurrent transfer from BET molecules to graphene through Zn<sub>0.9</sub>Mg<sub>0.1</sub>O nanoparticles and quickly spread in the graphene, producing a short transit time. The leftover holes residing in BET molecules are blocked by the Zn<sub>0.9</sub>Mg<sub>0.1</sub>O nanoparticles from recombination with electrons in graphene and hence enjoy a long carrier lifetime. Taking the measured noise current at 1 Hz as  $1.08 \times 10^{-10}$  A Hz<sup>-1/2</sup>, the measured detectivity reaches up to  $1.7 \times 10^{12}$  Jones. The high detectivity is one of the key advantages of our narrowband photodetector design.

In the organic dye family, there are thousands of dye molecules with different kinds and numbers of chromophore groups and their complexes,<sup>[45,46]</sup> which could be compatibly used in our method not only for narrowband photodetection but also to customize the responsive spectra. Here, we demonstrated the construction of a sensitive photodetector with customized responsive spectrum by using N4 dye as the light absorber. The N4 molecule is a 9,9-dihexyl-9H-fluorene functionalized zinc porphyrin dye, whose structure is displayed in the inset of Figure 3a. The carboxylic acid group of N4 molecule prompts its binding to Zn<sub>0.9</sub>Mg<sub>0.1</sub>O nanoparticles. The absorption spectrum in Figure 3a shows that N4 molecules on Zn<sub>0.9</sub>Mg<sub>0.1</sub>O nanoparticles layer have two narrowband

absorption peaks at 460 and 660 nm, corresponding to two chromophore groups of N4 molecule as shown in the inset of Figure 3a. This narrowband absorption also implies that N4 dyes anchored on the Zn<sub>0.9</sub>Mg<sub>0.1</sub>O nanoparticles are isolated instead of coupling to each other. As shown in Figure 3b, the nearly complete PL quenching indicates high efficiency of photogenerated charge transfer from N4 molecule to Zn<sub>0.9</sub>Mg<sub>0.1</sub>O nanoparticles, in analogy to the BET case (Figure S12, Supporting Information). We believe that we thus have built, for the first time, a dual-band narrowband photodetector based on our N4 dyes (Figure 3c,d). One detectable band is from 400 to 500 nm (FWHM  $\approx$  50 nm), and the other detectable band is from 610 to 700 nm (FWHM  $\approx$  45 nm). The first responsivity (EQE) peak reaches up to  $6.5 \times 10^3$  A W<sup>-1</sup> ( $1.75 \times 10^4$ ) at 460 nm, and the second responsivity (EQE) peak is about  $1.73 \times 10^3$  A W<sup>-1</sup> ( $3.66 \times 10^3$ ) at 660 nm. In comparison, the N4/graphene photodetector presents broadband photodetection with lower responsivity, as the resonance between N4 molecule and graphene and N4 molecule aggregation broadens the response spectrum. Such a dual-band photoresponse is unique as compared to other narrowband photodetectors. Two detectivity peaks are obtained as  $1.3 \times 10^{12}$  Jones at 460 nm and  $4 \times 10^{11}$  Jones at 660 nm, which are comparable with that of other narrowband photodetectors. In principle, we could customize the responsive spectrum of our dye-based

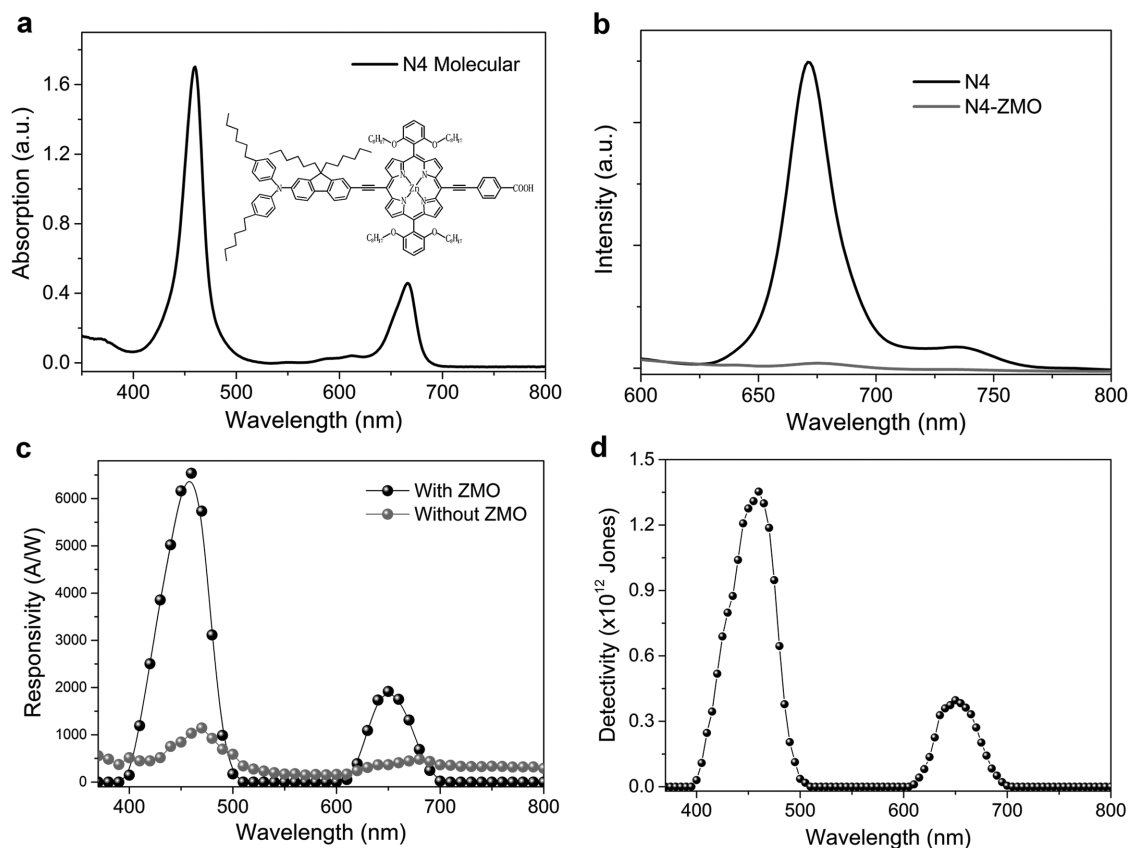


**Figure 3.** Narrowband photodetection of NZG device. a) Typical absorption of N4 molecules on the Zn<sub>0.9</sub>Mg<sub>0.1</sub>O nanoparticles layer. The inset is the structure of N4 molecule anchored on Zn<sub>0.9</sub>Mg<sub>0.1</sub>O nanoparticle. b) PL spectra of N4 molecules and on the Zn<sub>0.9</sub>Mg<sub>0.1</sub>O nanoparticles layer. c) Responsivity as a function of incident wavelength based on the N4/graphene device (gray dots) and the NZG device (black dots). d) Wavelength-dependent detectivity of the NZG device.

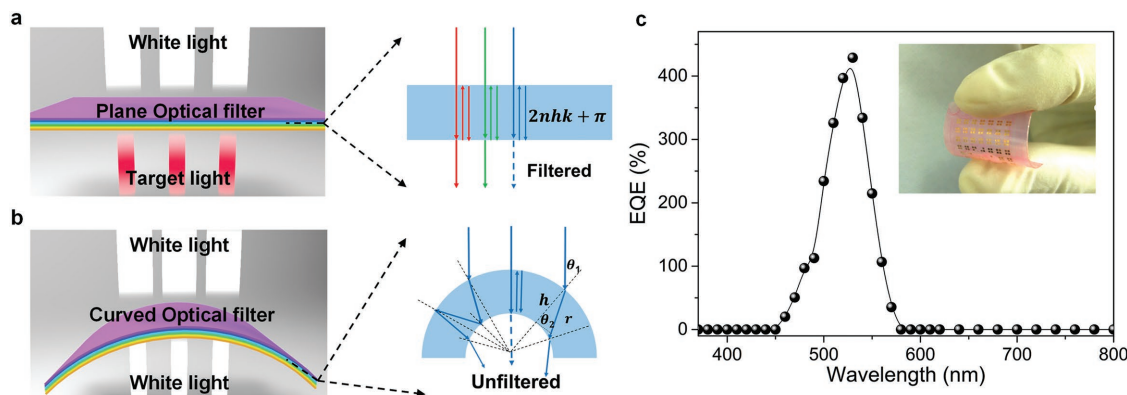


**Figure 4.** Flexible BZG narrowband photodetector. Schematic of white light through a) plane and b) curved multilayer interference filter and the optical path in one blue filter layer. c) Narrowband EQE of the BZG device at curved state. The inset is the curved BZG device. The channel length is 200  $\mu\text{m}$  and the width is 1 mm.

photodetectors, either single band or dual band or even multiple bands, simply by choosing different dyes absorbing in the target spectrum. Luckily, the two-decade intensive research in dye-sensitized solar cells has accumulated a large pool of organic dyes that are not only strong narrowband absorber but also could easily bind to  $\text{Zn}_{0.9}\text{Mg}_{0.1}\text{O}$  nanoparticles. Our work thus opens a new door to engineer sensitive narrowband photodetectors with customized detection ranges.

One additional advantage of our BZG photodetectors is their excellent flexibility. In order to meet the requirements for electronic skin<sup>[47,48]</sup> and flexible electronics<sup>[49,50]</sup> applications, flexible narrowband sensing and imaging are in urgent need, such as in bionic compound eyes.<sup>[51]</sup> It is challenging for commercial narrowband photodetectors to achieve flexible detection, because they rely on a precise multilayer filter to realize band-pass narrowband photodetection, as shown in Figure 4a,b. When the filter is flat, the thickness of these functional layers is well engineered so that the OPD of one light within the films is at odd times of its wavelength and would be filtered out. However, when the filter is bent, even to a small angle, the optical path difference of the target light would be totally ruined. What is worse, the change in optical path is nonlinear and highly sensitive to the wavelength and position of incident light, making the post-remedy almost impossible. As a result, the interference filter-based narrowband photodetection would be out of function when employed for flexible application. In contrast, our BZG photodetectors could be built on the PET substrate, use flexible graphene as the charge transfer channel, and employ no optical filter. As shown in Figure 4c, after bending, our BZG photodetector shows negligible degradation in device performance: the peak EQE reaches up to 420% at 530 nm, and the FWHM is about 50 nm. We further measured the device performance under different bending angles, as well as after 1000 times of 30° bending, and no degradation in device sensitivity was observed (Figures S14 and S15, Supporting Information). The preservation of narrowband photodetection is advantageous compared to the single-crystalline perovskite photodetectors and detectors employing optical filter, thus demonstrating the competitiveness of our BZG detectors for applications where flexibility is compulsory.

### 3. Conclusion

In conclusion, we have introduced a general strategy to employ organic dyes as sensitizers to achieve a sensitive narrowband photodetection compatible with flexible electronics. Our approach relies on a controlled adsorption of organic dyes onto the  $\text{Zn}_{0.9}\text{Mg}_{0.1}\text{O}$  nanoparticles in such a way that dye–dye coupling and  $\pi$ -resonances are suppressed, thereby maintaining the intrinsic narrowband character of the photosensitizer dyes. We further coupled these sensitized nanoparticles to a graphene substrate so that photogenerated charges could be transferred from dyes to graphene and then efficiently collected by the electrodes. Using this architecture, we implemented a BZG hybrid photodetector with an FWHM of 60 nm, a responsivity of  $8 \times 10^3 \text{ A W}^{-1}$ , and a detectivity of  $1.7 \times 10^{12}$  Jones. This represents an increase in responsivity over four orders of magnitude compared to the best reported narrowband photodetectors under the comparable electric field. We also demonstrated the broad application of this architecture and achieved dual-band narrowband photodetection using N4 dye as a sensitizer. Our approach does not rely on optical filters and is compatible with flexible and wearable electronics. Considering the rich options of organic dyes in nature and from synthetic chemistry, we believe that our strategy provides a new powerful way for narrowband photodetection with easy integration, tunable responsive spectrum, and high sensitivity, which is particularly competitive for flexible narrowband photodetection.

### 4. Experimental Section

**Material Synthesis:** The graphene on copper foil was grown through a modified CVD method. BET and N4 were synthesized by the reported methods.<sup>[30,52]</sup>  $\text{Zn}_{0.9}\text{Mg}_{0.1}\text{O}$  nanoparticles were synthesized as following: 0.297 g zinc acetate and 0.0321 g magnesium acetate were dissolved in 15 mL dimethyl sulfoxide (DMSO), respectively. The uniform solution containing 0.462 g tetramethyl ammonium hydroxide and 5 mL ethanol was slowly dropped into the fully dissolved DMSO. The stock was acquired after the mixture stirred at 30 °C for 12 h. Ten milliliter ethyl acetate was added into 5 mL stock to get the suspension liquid. Then, it was centrifuged at 5000  $\text{r min}^{-1}$  to precipitate  $\text{Zn}_{0.9}\text{Mg}_{0.1}\text{O}$  nanoparticles.

The  $Zn_{0.9}Mg_{0.1}O$  nanoparticles were dispersed in 2.5 mL ethanol for further application.

**Device Fabrication:** The few-layer graphene grown on copper foil was fixed on a clean white glass. Two layers of PMMA were spin-coated on it at a  $2500 \text{ r min}^{-1}$  speed. Then, the sample was baked for 2 min on the hot plate to promote the adhesion of PMMA and graphene. The backside graphene on copper foils was removed by  $O_2$  plasma at  $200 \text{ }^\circ\text{C}$  for 30 s. After etching copper foil with  $0.2 \text{ mol L}^{-1}$  nitric acid aqueous solution, graphene and PMMA were transferred onto a clean  $SiO_2/Si$  or PET substrate. PMMA on the graphene surface was dissolved with  $60 \text{ }^\circ\text{C}$  acetone. The 80 nm thick Au electrodes patterned by metallic mask were deposited on graphene by regular thermal evaporation. Three layers of  $Zn_{0.9}Mg_{0.1}O$  nanoparticles were spin-coated on graphene, and every layer was baked at  $70 \text{ }^\circ\text{C}$  for 2 min. Then, the  $Zn_{0.9}Mg_{0.1}O$ /graphene device was immersed in a BET toluene solution or N4 methanol DMF hybrid solution (optimization in Figure S13 in the Supporting Information) for 30 min to promote dye absorption. The device was rinsed by toluene or methanol to remove physically adsorbed dye molecule and then encapsulated by PMMA through the spin-coating method.

**Photoelectric Performance Characterization:** All device performance characterizations were done in an optically and electrically sealed box to minimize an electromagnetic disturbance. Three monochromatic light sources for photoresponse testing were a 530 nm LED (Thorlabs M530L3), a 410 nm LED, and a 780 nm LED (Thorlabs M780L3) modulated by a waveform generator (Agilent 33600A Series). For the wavelength-dependent photocurrent measurement, the spectrum was generated by modulating a bromine tungsten lamp using optical grating with a minimum interval of 0.1 nm. Current–voltage characteristic, transient response, and narrowband photodetection were measured using a semiconductor device analyzer (Agilent B1500A) by averaging the current over time for each voltage step. The noise current was measured using a lock-in (Stanford 850). We connected a standard resistor with our device and a 1.5 V battery. The standard resistor had the same resistance with our device to input voltage signal to a lock-in amplifier. The lock-in amplifier provided a scanning reference frequency to collect the frequency-dependent voltage signal, which was used to calculate the frequency-dependent noise current in  $\text{A Hz}^{-1/2}$ . Detectivity is calculated as  $D^* = R\sqrt{A}/i_n$ , where  $R$  is the responsivity,  $A$  is the device active area,  $f$  is the frequency bandwidth, and  $i_n$  is the noise current. The responsivity is calculated by the equation  $R = (I_p - I_D)/P_{in}$ , where  $P_{in}$  is the incident light power, the product of incident light power density and active area of the device. We chose 1 Hz for  $f$  as this is the 3 dB bandwidth of our device. Taking the measured noise current at 1 Hz as  $1.08 \times 10^{-10} \text{ A Hz}^{-1/2}$  in Figure 2f, the detectivity is calculated.

## Supporting Information

Supporting Information is available from the Wiley Online Library or from the author.

## Acknowledgements

L.G. and C.G. contributed equally to this work. This work was supported by the Major State Basic Research Development Program (2016YFB0700700 and 2016YFA0204000), the seed project of the Wuhan National Laboratory for Optoelectronics, and the Self-determined and Innovative Research Funds of the HUST (2016JCTD111). The authors thank the Analytical and Testing Center of the HUST and the Optoelectronic Micro-Nanoelectronic Manufacturing Process Platform of the WNLO for the characterization support.

## Conflict of Interest

The authors declare no conflict of interest.

## Keywords

flexible electronics, high sensitivity photodetectors, narrowband photodetectors, organic dyes

Received: May 2, 2017

Revised: May 25, 2017

Published online:

- [1] G. Konstantatos, E. H. Sargent, *Nat. Nanotechnol.* **2010**, *5*, 391.
- [2] S. Assefa, F. Xia, Y. A. Vlasov, *Nature* **2010**, *464*, 80.
- [3] I. L. Medintz, H. T. Uyeda, E. R. Goldman, H. Mattoussi, *Nat. Mater.* **2005**, *4*, 435.
- [4] C.-H. Liu, Y.-C. Chang, T. B. Norris, Z. Zhong, *Nat. Nanotechnol.* **2014**, *9*, 273.
- [5] Q. Bao, K. P. Loh, *ACS Nano* **2012**, *6*, 3677.
- [6] L. Gao, C. Chen, K. Zeng, C. Ge, D. Yang, H. Song, J. Tang, *Light: Sci. Appl.* **2016**, *5*, e16126.
- [7] A. Sobhani, M. W. Knight, Y. Wang, B. Zheng, N. S. King, L. V. Brown, Z. Fang, P. Nordlander, N. J. Halas, *Nat. Commun.* **2013**, *4*, 1643.
- [8] Y. Fang, Q. Dong, Y. Shao, Y. Yuan, J. Huang, *Nat. Photonics* **2015**.
- [9] C.-C. Chang, Y. D. Sharma, Y.-S. Kim, J. A. Bur, R. V. Shenoi, S. Krishna, D. Huang, S.-Y. Lin, *Nano Lett.* **2010**, *10*, 1704.
- [10] M. Dandin, P. Abshire, E. Smela, *Lab Chip* **2007**, *7*, 955.
- [11] G. Olbright, N. Peyghambarian, H. Gibbs, H. Macleod, F. Van Milligen, *Appl. Phys. Lett.* **1984**, *45*, 1031.
- [12] H. Park, Y. Dan, K. Seo, Y. J. Yu, P. K. Duane, M. Wober, K. B. Crozier, *Nano Lett.* **2014**, *14*, 1804.
- [13] E. Cicek, R. McClintock, C. Cho, B. Rahnema, M. Razeghi, *Appl. Phys. Lett.* **2013**, *103*, 191108.
- [14] X. Wang, K. Liu, X. Chen, B. Li, M. Jiang, Z. Zhang, H. Zhao, D. Shen, *ACS Appl. Mater. Interfaces* **2017**, *9*, 5574.
- [15] Y. J. Fang, Q. F. Dong, Y. C. Shao, Y. B. Yuan, J. S. Huang, *Nat. Photonics* **2015**, *9*, 679.
- [16] Q. Lin, A. Armin, P. L. Burn, P. Meredith, *Nat. Photonics* **2015**, *9*, 687.
- [17] A. Armin, R. D. Jansen-van Vuuren, N. Kopidakis, P. L. Burn, P. Meredith, *Nat. Commun.* **2015**, *6*, 6343.
- [18] W. Wang, F. Zhang, M. Du, L. Li, M. Zhang, K. Wang, Y. Wang, B. Hu, Y. Fang, J. Huang, *Nano Lett.* **2017**, *17*, 1995.
- [19] D. M. Lyons, A. Armin, M. Stolterfoht, R. C. Nagiri, R. D. Jansen-van Vuuren, B. N. Pal, P. L. Burn, S.-C. Lo, P. Meredith, *Org. Electron.* **2014**, *15*, 2903.
- [20] K.-H. Lee, G. H. Lee, D.-S. Leem, J. Lee, J. W. Chung, X. Bulliard, H. Choi, K.-B. Park, K.-S. Kim, Y. W. Jin, *J. Phys. Chem. C* **2014**, *118*, 13424.
- [21] A. Hagfeldt, G. Boschloo, L. Sun, L. Kloo, H. Pettersson, *Chem. Rev.* **2010**, *110*, 6595.
- [22] D. Bagnis, L. Beverina, H. Huang, F. Silvestri, Y. Yao, H. Yan, G. A. Pagani, T. J. Marks, A. Facchetti, *J. Am. Chem. Soc.* **2010**, *132*, 4074.
- [23] Y. Wu, W. Zhu, *Chem. Soc. Rev.* **2013**, *42*, 2039.
- [24] A. Tsuda, A. Osuka, *Science* **2001**, *293*, 79.
- [25] Y. Lee, S. H. Yu, J. Jeon, H. Kim, J. Y. Lee, H. Kim, J.-H. Ahn, E. Hwang, J. H. Cho, *Carbon* **2015**, *88*, 165.
- [26] C. J. Raj, K. Prabakar, S. Karthick, K. Hemalatha, M.-K. Son, H.-J. Kim, *J. Phys. Chem. C* **2013**, *117*, 2600.
- [27] J. Rochford, D. Chu, A. Hagfeldt, E. Galoppini, *J. Am. Chem. Soc.* **2007**, *129*, 4655.
- [28] E. Palomares, J. N. Clifford, S. A. Haque, T. Lutz, J. R. Durrant, *J. Am. Chem. Soc.* **2003**, *125*, 475.

- [29] J. Qi, X. Dang, P. T. Hammond, A. M. Belcher, *ACS Nano* **2011**, 5, 7108.
- [30] M. Shrestha, L. Si, C.-W. Chang, H. He, A. Sykes, C.-Y. Lin, E. W.-G. Diau, *J. Phys. Chem. C* **2012**, 116, 10451.
- [31] Z. Ning, Y. Fu, H. Tian, *Energy Environ. Sci.* **2010**, 3, 1170.
- [32] Y. Zhao, Y. Xie, Z. Bao, Y. H. Tsang, L. Xie, Y. Chai, *J. Phys. Chem. C* **2014**, 118, 11827.
- [33] B. E. Hardin, E. T. Hoke, P. B. Armstrong, J.-H. Yum, P. Comte, T. Torres, J. M. Fréchet, M. K. Nazeeruddin, M. Grätzel, M. D. McGehee, *Nat. Photonics* **2009**, 3, 406.
- [34] C. Jia, J. Jiang, L. Gan, X. Guo, *Sci. Rep.* **2012**, 2, 707.
- [35] C. Y. Lee, J. T. Hupp, *Langmuir* **2009**, 26, 3760.
- [36] Y.-C. Chang, C.-L. Wang, T.-Y. Pan, S.-H. Hong, C.-M. Lan, H.-H. Kuo, C.-F. Lo, H.-Y. Hsu, C.-Y. Lin, E. W.-G. Diau, *Chem. Commun.* **2011**, 47, 8910.
- [37] F. Lenzmann, J. Krueger, S. Burnside, K. Brooks, M. Grätzel, D. Gal, S. Rühle, D. Cahen, *J. Phys. Chem. B* **2001**, 105, 6347.
- [38] S. Das, H.-Y. Chen, A. V. Penumatcha, J. Appenzeller, *Nano Lett.* **2012**, 13, 100.
- [39] J. O. Island, S. I. Blanter, M. Buscema, H. S. van der Zant, A. Castellanos-Gomez, *Nano Lett.* **2015**, 15, 7853.
- [40] O. Lopez-Sanchez, D. Lembke, M. Kayci, A. Radenovic, A. Kis, *Nat. Nanotechnol.* **2013**, 8, 497.
- [41] N. C. Greenham, X. Peng, A. P. Alivisatos, *Phys. Rev. B* **1996**, 54, 17628.
- [42] S. A. McDonald, G. Konstantatos, S. Zhang, P. W. Cyr, E. J. Klem, L. Levina, E. H. Sargent, *Nat. Mater.* **2005**, 4, 138.
- [43] Z. Sun, Z. Liu, J. Li, G. a. Tai, S. P. Lau, F. Yan, *Adv. Mater.* **2012**, 24, 5878.
- [44] G. Konstantatos, I. Howard, A. Fischer, S. Hoogland, J. Clifford, E. Klem, L. Levina, E. H. Sargent, *Nature* **2006**, 442, 180.
- [45] M. Grätzel, *Acc. Chem. Res.* **2009**, 42, 1788.
- [46] W. M. Campbell, K. W. Jolley, P. Wagner, K. Wagner, P. J. Walsh, K. C. Gordon, L. Schmidt-Mende, M. K. Nazeeruddin, Q. Wang, M. Grätzel, *J. Phys. Chem. C* **2007**, 111, 11760.
- [47] M. L. Hammock, A. Chortos, B. C. K. Tee, J. B. H. Tok, Z. Bao, *Adv. Mater.* **2013**, 25, 5997.
- [48] G. Schwartz, B. C.-K. Tee, J. Mei, A. L. Appleton, D. H. Kim, H. Wang, Z. Bao, *Nat. Commun.* **2013**, 4, 1859.
- [49] S. Bauer, *Nat. Mater.* **2013**, 12, 871.
- [50] A. Nathan, A. Ahnood, M. T. Cole, S. Lee, Y. Suzuki, P. Hiralal, F. Bonaccorso, T. Hasan, L. Garcia-Gancedo, A. Dyadyusha, *Proc. IEEE* **2012**, 100, 1486.
- [51] K.-H. Jeong, J. Kim, L. P. Lee, *Science* **2006**, 312, 557.
- [52] W. Li, L. Si, Z. Liu, Z. Zhao, H. He, K. Zhu, B. Moore, Y.-B. Cheng, *J. Mater. Chem. A* **2014**, 2, 13667.